

Nanoindentation Behaviour of As-Deposited and Annealed CuO/GaAs Thin Films

Woei-Shyan Lee* and Chia-Yuan Chang **

Keywords: Nanoindentation, GaAs, Microstructural evolution, Annealing, CuO thin films.

ABSTRACT

CuO thin films with thicknesses of 200 nm and 300 nm, respectively, are deposited on GaAs substrates. The mechanical properties of the CuO/GaAs thin-film systems are evaluated under room temperature conditions by nanoindentation tests performed to depths ranging from 150 to 350 nm. The tests are performed using both as-deposited samples and samples annealed at 500°C for 30 minutes. The results show that for the as-deposited specimens, a pop-in effect occurs in the loading curve for all film thicknesses and nanoindentation depths (150 nm, 250 nm and 350 nm) due to a delamination of the thin film from the substrate. However, for the annealed samples, no pop-in events are observed, irrespective of the film thickness or nanoindentation depth. For both samples (as-deposited and annealed), the maximum indentation load increases with an increasing indentation depth and film thickness. However, the shape of the hardness-depth curve for the annealed specimens is different from that of the as-deposited specimens. Moreover, the hardness of the annealed specimens is less than that of the as-deposited specimens at the maximum indentation depth. Similar tendencies are observed for the variation of the Young's modulus with the indentation depth. Scanning electron microscopy (SEM) observations show that the indentation area increases with an increasing indentation depth and thin film thickness, but decreases in the annealed condition. Furthermore, the transmission electron microscopy (TEM) observations reveal that no delamination occurs for the annealed specimen with the maximum thickness of 300 nm under

indentation depths of 150 nm and 350 nm. In addition, dislocations within the GaAs substrate are apparent only in the annealed specimen with a thickness of 300 nm and an indentation depth of 350 nm. The selected area (electron) diffraction (SAED) patterns confirm that the as-deposited and annealed CuO film has a polycrystalline structure, while the GaAs substrate has a single crystal structure. Finally, the high-resolution TEM (HRTEM) micrographs show that the as-deposited and annealed CuO film and GaAs substrate have lattice spacings of 0.25 nm and 0.283 nm, respectively.

INTRODUCTION

Gallium arsenide (GaAs) has a high electron mobility and drift velocity, a high bandgap, and good thermal stability. As a result, it is widely used in the fabrication of displays, sensors, light-emitting diodes (LEDs), and solar cells (Yugang *et al.*, 2005; Nakamura, 2012). For solar cell applications, the deposition of a thin layer of CuO on the GaAs surface improves the solar energy absorption efficiency and minimizes the thermal emittance (Yatendra *et al.*, 2004; Electrochem, 2011; Nau-Hung Tsao, 2011). However, to ensure the robustness of the CuO/GaAs structure during the panel fabrication process, the mechanical properties of the CuO/GaAs thin-film system must be properly understood.

The literature contains many studies on the mechanical properties of GaAs during nanoindentation. In general, these studies have shown that GaAs undergoes plastic deformation under the effects of the indentation load (Leipner *et al.*, 2001). However, the effects of the annealing temperature on the plastic deformation of nanoindented CuO/GaAs thin films are still not clear. Many studies have shown the existence of a discontinuity (pop-in) phenomenon in the loading curve of GaAs and other semiconductors (Leipner *et al.*, 2001; Chrobak *et al.*, 2007). Furthermore, a pop-out phenomenon has also been observed in the unloading curve of crystalline silicon and relaxed amorphous silicon (Rao *et al.*, 2007). These discontinuities have been variously ascribed to the deformation of dislocations, plastic deformation, and buckling phenomena under the action of the indenter (Patriarche *et al.*, 2004). For solar cell

Paper Received January 2020. Revised February, 2020. Accepted March, 2020. Author for Correspondence: Woei-Shyan Lee.

* Distinguished Professor, Department of Mechanical Engineering, National Cheng Kung University, Tainan, Taiwan 70101, ROC.

** Graduate Student, Department of Mechanical Engineering, National Cheng Kung University, Tainan, Taiwan 70101, ROC.

applications, the structural discontinuities may result in significant changes to the mechanical and electrical properties. Consequently, the origins and effects of these discontinuities must be properly understood. Accordingly, the present study investigates the mechanical properties (i.e., hardness and Young's modulus) of two CuO/GaAs thin-film systems with thicknesses of 200 nm and 300 nm, respectively, under nanoindentation depths in the range of 150 to 350 nm.

The nanoindentation tests are performed using both as-deposited samples and specimens annealed at a temperature of 500°C for 30 minutes. The effects of the thin-film thickness, indentation depth and annealing process on the mechanical properties of the CuO/GaAs thin films are clarified by means of scanning electron microscopy (SEM) and transmission electron microscopy (TEM) observations. Finally, the crystal structures and lattice spacings of the as-deposited and annealed nanoindented CuO/GaAs structures are examined via selected area (electron) diffraction (SAED) analysis and high-resolution TEM (HRTEM).

THEORETICAL BACKGROUND OF NANOINDENTATION TESTS

In nanoindentation tests, the Young's modulus is generally evaluated using the Oliver and Pharr model, which has the form (Timoshenko and Goodier, 1951; Pharr *et al.*, 1992)

$$\frac{1}{E_r} = \frac{(1-\nu_s^2)}{E_s} + \frac{(1-\nu_i^2)}{E_i} \quad (1)$$

where E_s and E_i are the elastic modulus values of the specimen and indenter, respectively; ν_s and ν_i are the Poisson ratios of the specimen and indenter, respectively; and E_r is the reduced modulus, which accounts for the elastic deformation of the indenter, and is defined as

$$E_r = \frac{\sqrt{\pi}}{2} \frac{S}{\sqrt{A}} \quad (2)$$

where S is the contact stiffness (i.e., the slope of the load-displacement curve at the beginning of the unloading phase) and A is the projected contact area. The contact stiffness is derived as

$$S = \left. \frac{dP}{dh} \right|_{h_{max}} \quad (3)$$

where h is the total displacement of the probe centre from the surface. Defining h_c as the contact depth, i.e., the vertical depth over which the probe contacts the specimen, and h_s as the surface depth, i.e., the vertical depth over which the probe does not contact the surface, h can be defined mathematically as

$$h = h_s + h_c \quad (4)$$

Under the assumption of elastic deformation, the loading force and probe displacement during the

unloading stage are related by the following power law equation:

$$P = \alpha(h - h_f)^m \quad (5)$$

Where P is the loading force, $h - h_f$ is the elastic displacement of the probe, and α and m are constants derived by curve fitting the following equation:

$$S = \left(\frac{dP}{dh} \right)_{h_{max}} = \alpha m (h_{max} - h_f)^{m-1}$$

(6).

The hardness of the sample can be obtained by dividing the maximum normal indentation load, P_{max} by the projected area of the contact depth A , i.e.,

$$H = \frac{P_{max}}{A} \quad (7)$$

where A is determined from the area function $A(h_c)$, in which h_c is the actual depth of contact and is defined as

$$h_c = h_{max} - \varepsilon \frac{P_{max}}{S} \quad (8)$$

where h_{max} is the maximum penetration depth of the indenter, ε is a geometrical constant associated with the indenter shape (e.g., $\varepsilon = 0.75$ for a Berkovich indenter), and S is the contact stiffness.

Having computed h_c , the projected contact area A can be determined from the following fitting equation (Oliver and Pharr, 1992)

$$A = f(h_c) = 24.5h_c^2 + c_1h_c^1 + c_2h_c^{1/2} + c_3h_c^{1/4} + \dots + c_8h_c^{1/128} \quad (9)$$

where C_1 through C_8 are constants. Note that the first term on the right-hand side of Eq. (9) describes a perfect Berkovich indenter, while the other terms describe the deviations of the actual indenter geometry from the ideal Berkovich geometry due to tip blunting.

If the probe geometry is not axisymmetric, the reduced modulus given in Eq. (2) should be revised as follows:

$$E_r = \frac{1}{\beta} \frac{\sqrt{\pi}}{2} \frac{S}{\sqrt{A}} \quad (10)$$

where β has a value of 1.034 for a Berkovich probe (Hansen and Anderko, 1958)

CuO/GaAs thin films are single-film coated systems with a composite structure. Consequently, the Young's modulus of the film is determined by both the Young's modulus of the CuO film and the Young's modulus of the GaAs substrate. In other words, the Young's modulus E_f of the combined film/substrate system can be estimated as (Huajian *et al.*, 1992)

$$\frac{1}{E_r} = \frac{1-\nu_i^2}{E_i} + \frac{1-\nu_f^2}{E_f} (1 - e^{-\frac{\alpha L}{a}}) + \frac{1-\nu_s^2}{E_s} e^{-\frac{\alpha L}{a}} \quad (11)$$

where E_s is the Young's modulus of the bulk gallium arsenide substrate, and E_r is the reduced modulus. Furthermore, V_s , V_i and V_f are the Poisson ratios of the specimen, indenter and film, respectively; and t is the depth under the indenter. Finally, $a = \sqrt{A}$ and α is a constant relating to the probe geometry.

EXPERIMENTAL PROCEDURE

TEM foils were prepared using a Hitachi NX2000 advanced triple focused ion beam (FIB) milling system with a Ga⁺ ion beam and an operation voltage of 30 keV (see Fig. 1). (Note that before the foils were milled, a thin film of carbon was deposited on the specimen surface to protect the indentation region from accidental damage by the ion beam. The cross-sectional microstructures of the various specimens were observed using an EOL JEM-3010 Analytical Scanning Transmission Microscope at 300 kV.

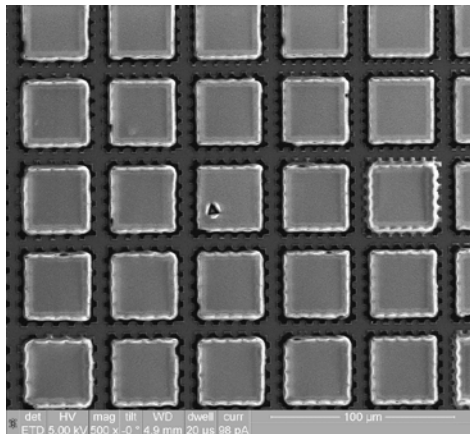


Fig. 1 (a) Original indentation positions identified using scanning electron microscopy and permanent position array system.

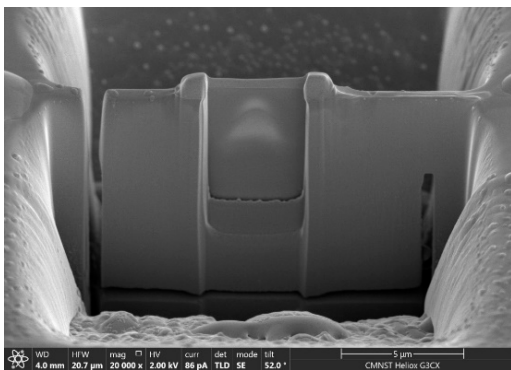


Fig. 1 (b) TEM thin foil specimen prepared using focused ion beam (FIB) milling system.

CuO/GaAs specimens were prepared by depositing CuO films with thicknesses of approximately 200 and 300 nm, respectively, on GaAs substrates using a RF-sputtering deposition system. During the deposition process, the substrate was

rotated at a speed of 250 rpm and maintained at a temperature of 200 °C in order to improve the uniformity of the deposited film. Following the deposition process, half of the specimens were annealed at 500 °C for 30 minutes in a thermal annealing system. Nanoindentation tests were then performed on both the as-deposited samples and the annealed samples using an MTS nanoindenter XP system with a Berkovich diamond pyramid tip. For each sample, the indentation procedure was performed using the following steps: (1) the specimen was indented to a maximum depth of 150 nm, 250 nm or 350 nm; (2) the indenter was held at the point of maximum indentation depth for 10s; and (3) the indenter was smoothly unloaded over a period of 15s. The load-displacement data recorded during each test were used to determine the hardness and Young's modulus of the CuO/GaAs thin film in accordance with the Oliver and Pharr method described in (Li and Bhushan, 2002).

RESULTS and DISCUSSION

Loading-unloading curves

Figures 2(a) and (b) show the load-unloading curves of the as-deposited and annealed specimens, respectively, with a thin film thickness of 200 nm and an indentation depth of 150 nm. For the as-deposited specimen (Fig. 2(a)), a clear pop-in event is seen in the loading curve. However, for the annealed specimen, no such effect is observed (Fig. 2(b)).

Figures 2(c) and (d) show the load-unloading curves of the as-deposited and annealed specimens with the same thin film thickness of 200 nm, but a greater indentation depth of 250 nm. Again, distinct pop-in events are observed in the loading curve of the as-deposited sample, but are absent in the annealed sample.

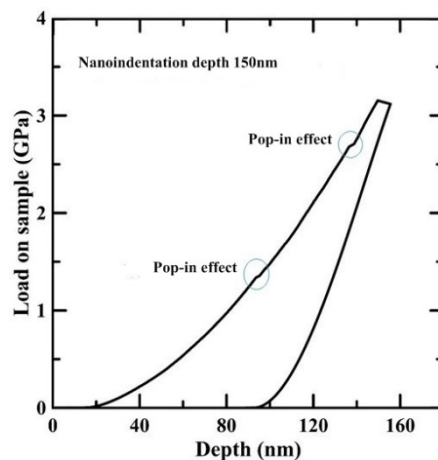


Fig. 2 (a) Load-displacement curves obtained in nanoindentation tests for as-deposited specimen with 200 nm thickness and indentation depth of 150 nm.

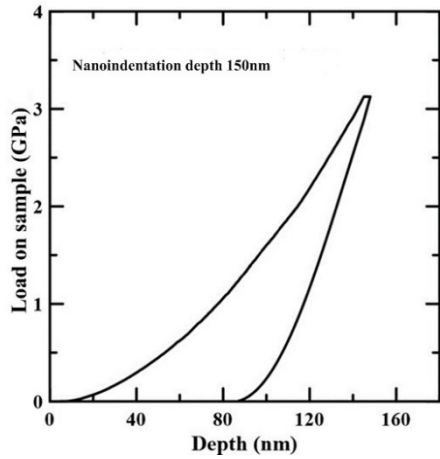


Fig. 2 (b) Load-displacement curves obtained in nanoindentation tests for annealed specimen with 200 nm thickness and indentation depth of 150 nm.

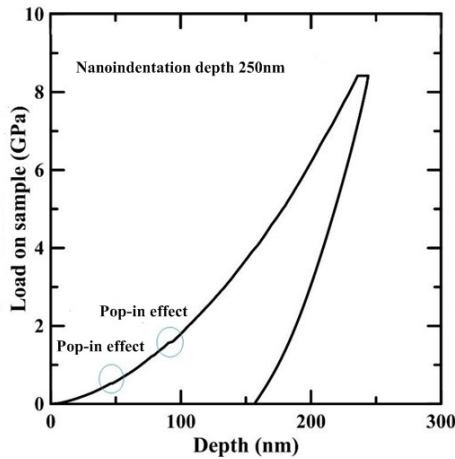


Fig. 2 (c) Load-displacement curves obtained in nanoindentation tests for as-deposited specimen with 200 nm thickness and indentation depth of 250 nm.

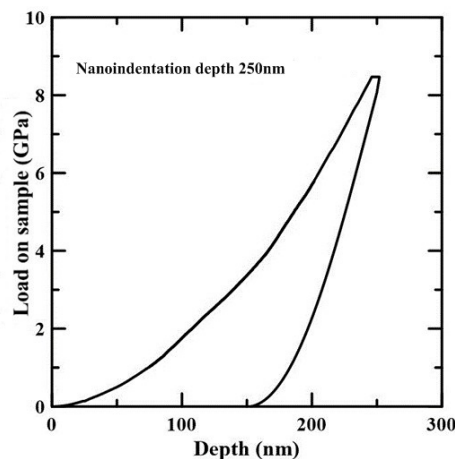


Fig. 2 (d) Load-displacement curves obtained in nanoindentation tests for annealed specimen with 200 nm thickness and indentation depth of 250 nm.

Figures 3(a) and (b) show the load-unloading curves of the as-deposited and annealed samples, respectively, with a thin film thickness of 300 nm and

an indentation depth of 150 nm. As for the cases shown in Fig. 2, the loading curves of the as-deposited samples show prominent pop-in features for both indentation depths.

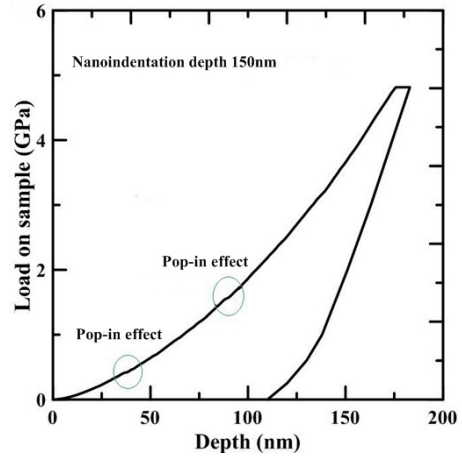


Fig. 3 (a) Load-displacement curves obtained in nanoindentation tests for as-deposited specimen with 300 nm thickness and indentation depth of 150 nm.

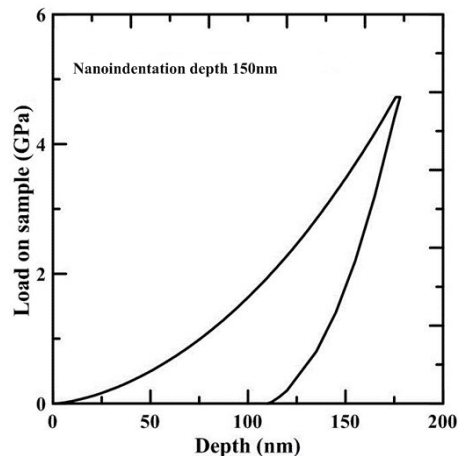


Fig. 3 (b) Load-displacement curves obtained in nanoindentation tests for annealed specimen with 300 nm thickness and indentation depth of 150 nm.

Figures 3(c) and (d) show the equivalent load-unloading curves for an indentation depth of 350 nm. for the annealed specimens, the loading curves are once again continuous and smooth without any pop-in events. The pop-in feature observed in the loading curves has been variously attributed to the generation of dislocations in the substrate (Wasmer *et al.*, 2011), a difference in the mechanical properties of the thin film and substrate, respectively (Haq *et al.*, 2007), and the formation of high pressure phase in the indentation process.

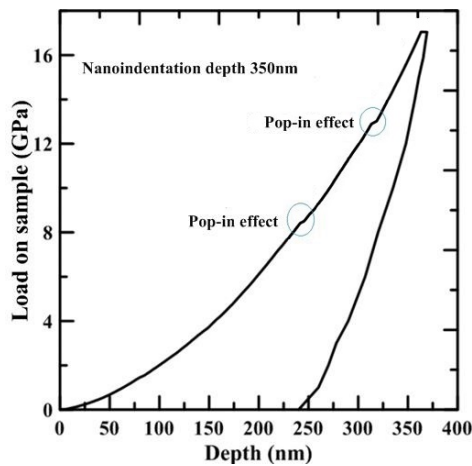


Fig. 3 (c) Load-displacement curves obtained in nanoindentation tests for as-deposited specimen with 300 nm thickness and indentation depth of 350 nm.

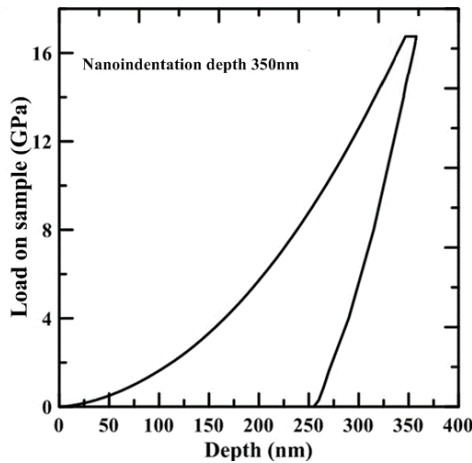


Fig. 3 (d) Load-displacement curves obtained in nanoindentation tests for annealed specimen with 300 nm thickness and indentation depth of 350 nm.

Comparing the various load-unloading curves shown in Figs. 2(a) to 3(d), it is seen that for a given thin film thickness, the maximum load increases with an increasing indentation depth. Similarly, for a constant indentation depth, the maximum load increases with an increasing thin film thickness.

Hardness of CuO/GaAs thin films

Figures 4(a) and (b) show the variation of the CuO/GaAs thin film hardness with the indentation depth for the as-deposited and annealed samples, respectively, with a film thickness of 200 nm and an indentation depth of 150 nm. For the as-deposited specimen (Fig. 4(a)), the hardness increases rapidly to a value of approximately 7.8 GPa during the initial indentation stage (i.e., a nanoindentation depth of less than 35 nm). Thereafter, the hardness increases slightly to a final value of around 8.2 GPa at the maximum indentation depth of 150 nm. The hardness-depth curve of the annealed specimen differs markedly

from that of the as-deposited sample. In particular, the hardness increases sharply to 7.8 GPa within just 12 nm (see Fig. 4(b)), but then reduces rapidly to approximately 6.3 GPa at an indentation depth of 31 nm. It then maintains a low and approximately constant value of 6 GPa as the indentation depth is further increased to 150 nm.

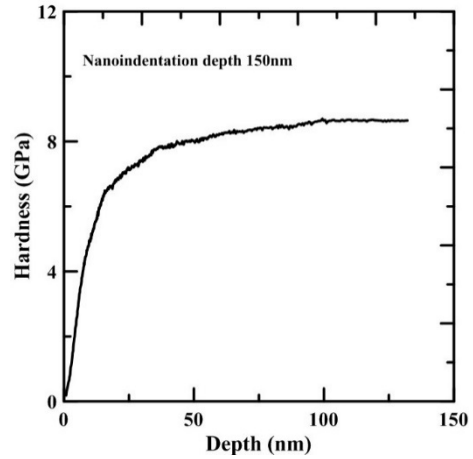


Fig. 4 (a) Hardness-displacement curves obtained in nanoindentation tests for as-deposited specimen with 200 nm thickness and indentation depth of 150 nm.

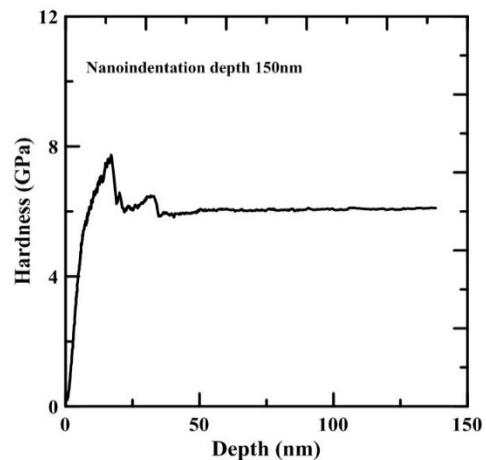


Fig. 4 (b) Hardness-displacement curves obtained in nanoindentation tests for annealed specimen with 200 nm thickness and indentation depth of 150 nm.

Figures 4(c) and (d) show the variation of the CuO/GaAs thin film hardness with the indentation depth for the as-deposited and annealed specimens, respectively, with a film thickness of 200 nm and an indentation depth of 250 nm. It is seen that for both samples, the shape and variation tendency of the hardness-depth curve are similar to those of the samples indented to a lower depth of 150 nm (Figs. 4(a) and (b)). Furthermore, the maximum hardness values of the two samples are also similar to those in Figs. 4(a) and (b).

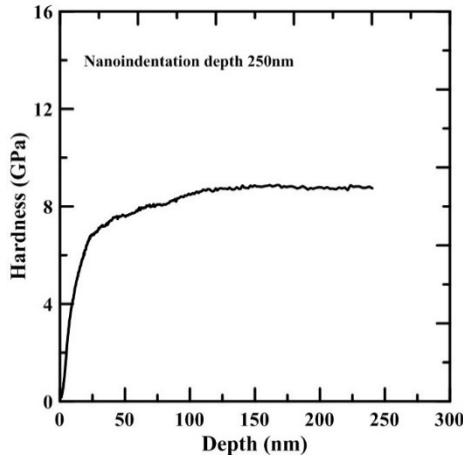


Fig. 4 (c) Hardness-displacement curves obtained in nanoindentation tests for as-deposited specimen with 200 nm thickness and indentation depth of 250 nm.

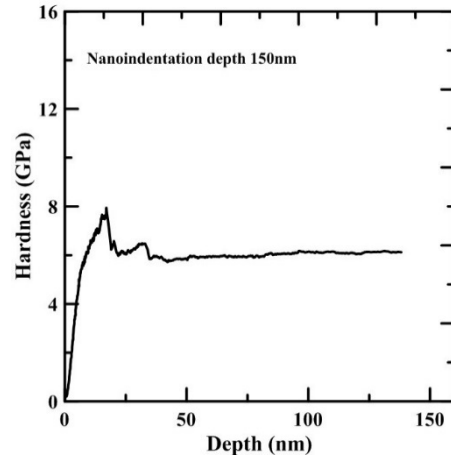


Fig. 5 (b) Hardness-displacement curves obtained in nanoindentation tests for annealed specimen with 300 nm thickness and indentation depth of 150 nm.

Figures 5(c) and (d) show the equivalent curves for the samples indented to a greater depth of 350 nm.

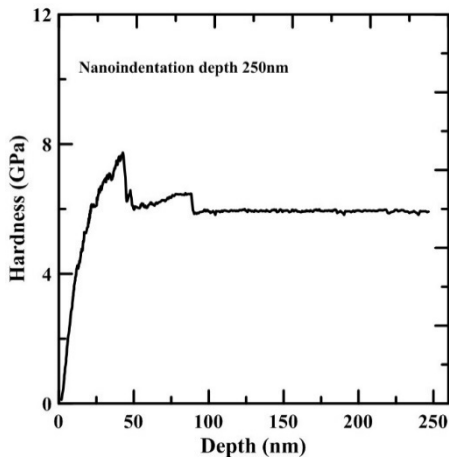


Fig. 4 (d) Hardness-displacement curves obtained in nanoindentation tests for annealed specimen with 200 nm thickness and indentation depth of 250 nm.

Figures 5(a) and (b) show the hardness-depth curves of the as-deposited and annealed samples with a thickness of 300 nm and indentation depth of 150 nm.

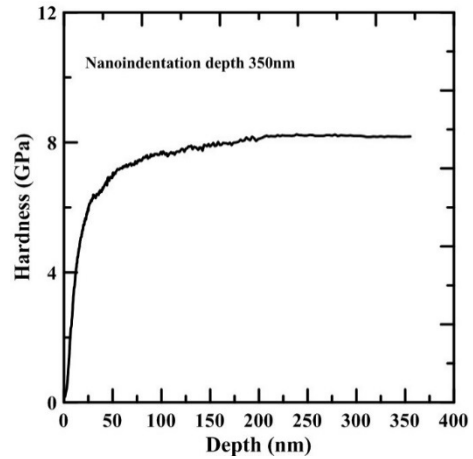


Fig. 5 (c) Hardness-displacement curves obtained in nanoindentation tests for as-deposited specimen with 300 nm thickness and indentation depth of 350 nm.

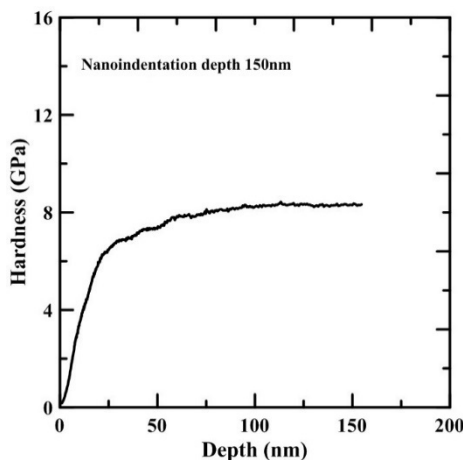


Fig. 5 (a) Hardness-displacement curves obtained in nanoindentation tests for as-deposited specimen with 300 nm thickness and indentation depth of 150 nm.

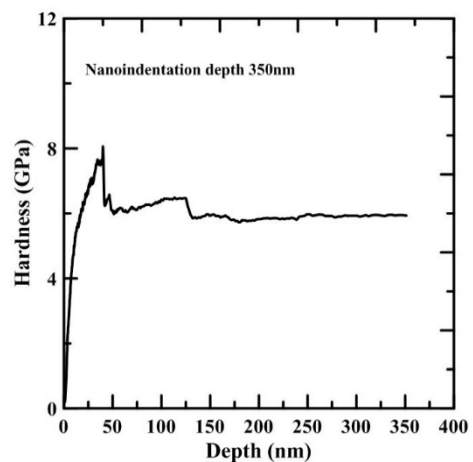


Fig. 5 (d) Hardness-displacement curves obtained in nanoindentation tests for annealed specimen with 300 nm thickness and indentation depth of 350 nm.

The maximum hardness values are again seen to be similar to those presented in Fig. 4 for the thin films with a lower thickness of 200 nm. Overall, therefore, the results presented in Figs. 4 and 5 show that the maximum hardness of the CuO/GaAs films is insensitive to both the indentation depth and the film thickness. However, for all values of the film thickness and indentation depth, the maximum hardness of the annealed samples is lower than that of the as-deposited samples.

Young's modulus of CuO/GaAs thin films

Figures 6(a) and (b) show the variation of the Young's modulus of the as-deposited specimen and annealed specimen, respectively, with a thickness of 200 nm and an indentation depth of 150 nm. For the as-deposited specimen (Fig. 6(a)), the Young's modulus has a value of approximately 40 GPa for indentation depths of less than 8 nm. However, as the indenter penetrates the CuO film slightly further, the Young's modulus decreases slightly to a value of 38 GPa due to the indentation size effect (Manika and Maniks, 2006) and a poorly-calibrated tip area function. As the indentation depth increases beyond 8 nm, the Young's modulus increases rapidly to a value of around 70 GPa at an indentation depth of 50 nm. It then increases slightly to a maximum value of 78 GPa as the indentation depth increases to 150 nm. For the annealed specimen (Fig. 6(b)), the oscillation effect caused by the poorly-calibrated tip area function occurs at a slightly higher indentation depth of 10 nm. As the indenter penetrates more deeply into the CuO film, the Young's modulus increases to a maximum value of approximately 78 GPa at an indentation depth of around 13 nm and then falls slowly to a constant value of around 64 GPa as the indentation depth is further increased to 150 nm.

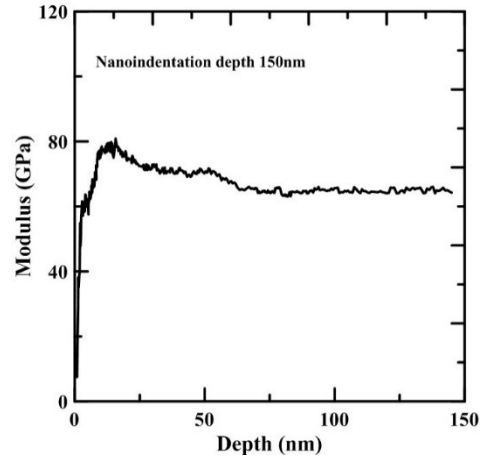


Fig. 6 (b) Modulus-displacement curves obtained in nanoindentation tests for annealed specimen with 200 nm thickness and indentation depth of 150 nm.

Figures 6(c) and (d) show the variation of the Young's modulus with the indentation depth for the samples with the same film thickness of 200 nm, but a higher indentation depth of 250 nm. The tendencies of the Young's modulus of the two samples are similar to those of the samples indented to a lower depth of 150 nm. In other words, for a constant film thickness, the Young's modulus is insensitive to the indentation depth. However, for both indentation depths, the Young's moduli of the annealed specimens are slightly lower than those of the as-deposited specimens.

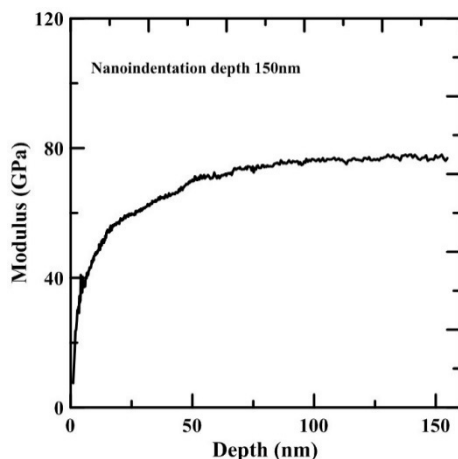


Fig. 6 (a) Modulus-displacement curves obtained in nanoindentation tests for as-deposited specimen with 200 nm thickness and indentation depth of 150 nm.

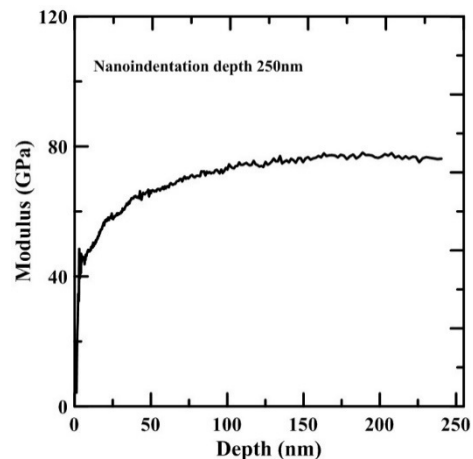


Fig. 6 (c) Modulus-displacement curves obtained in nanoindentation tests for as-deposited specimen with 200 nm thickness and indentation depth of 250 nm.

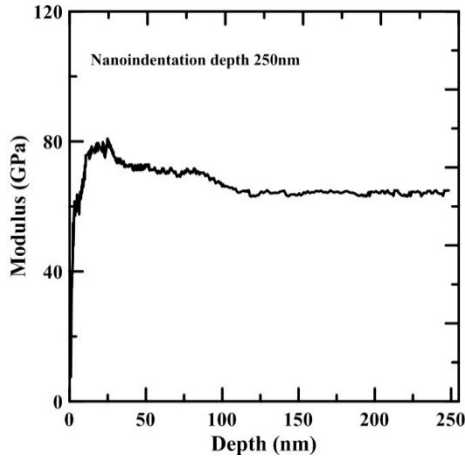


Fig. 6 (d) Modulus-displacement curves obtained in nanoindentation tests for annealed specimen with 200 nm thickness and indentation depth of 250 nm.

Figures 7(a) and (b) show the variation of the Young's modulus with the indentation depth for the as-deposited and annealed specimens, respectively, with a film thickness of 300 nm and an indentation depth of 150 nm.

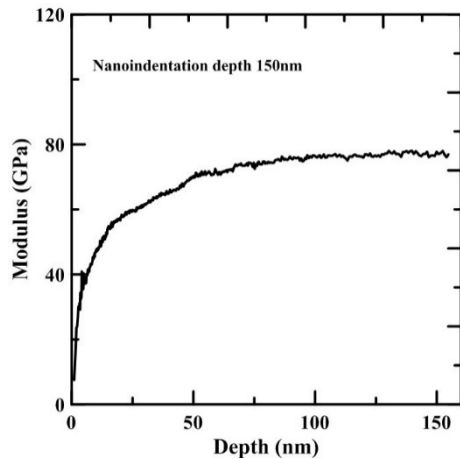


Fig. 7 (a) Modulus-displacement curves obtained in nanoindentation tests for as-deposited specimen with 300 nm thickness and indentation depth of 150 nm.

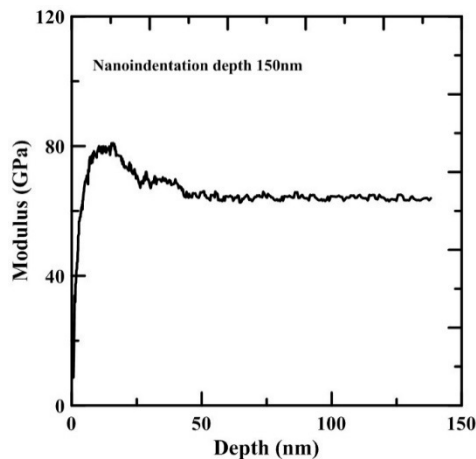


Fig. 7 (b) Modulus-displacement curves obtained in nanoindentation tests for annealed specimen with 300 nm thickness and indentation depth of 150 nm.

Figures 7(c) and (d) show the equivalent results for a higher indentation depth of 350 nm.

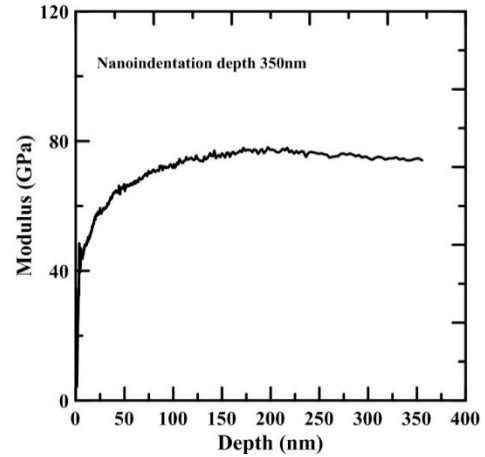


Fig. 7 (c) Modulus-displacement curves obtained in nanoindentation tests for as-deposited specimen with 300 nm thickness and indentation depth of 350 nm.

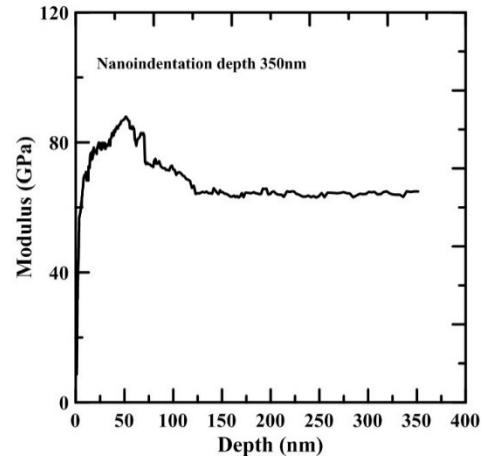


Fig. 7 (d) Modulus-displacement curves obtained in nanoindentation tests for annealed specimen with 300 nm thickness and indentation depth of 350 nm.

Figures 7(c) and (d) show the equivalent results for a higher indentation depth of 350 nm. The modulus profiles in Figs. 7(c) and (d) are similar to those in Figs. 7(a) and (b), respectively. In other words, for a thin film thickness of 300 nm, the Young's modulus is insensitive to the indentation depth. Moreover, the Young's modulus profiles shown in Fig. 7 for a thin film thickness of 300 nm are similar to those shown in Fig. 6 for a film thickness of 200 nm. In other words, the Young's modulus is also insensitive to the thin film thickness. However, for all of the samples, the annealing process results in a slight reduction in the Young's modulus

SEM analysis

Figures 8(a) and (b) present SEM surface topography images of the as-deposited and annealed specimens, respectively, with a film thickness of 200

nm and an indentation depth of 150 nm. It is observed that the indented zones have an approximately triangular shape and are free of cracking at the triangle corners. In other words, the CuO/GaAs thin film has a ductile property in both the as-deposited condition and the annealed condition (Cao *et al.*, 2006). However, comparing the two figures, it is seen that the annealed sample has a smaller indented zone, which suggests that the annealing process results in a greater degree of elastic spring-back.

Figures 8(c) and (d) show the surface topographies of the as-deposited and annealed specimens, respectively, with a film thickness of 200 nm and an indentation depth of 250 nm. For both specimens, the indented zone again has a triangular appearance with no cracks. Furthermore, the size of the indented zone in the annealed sample is again smaller than that in the as-deposited sample.

Comparing the images in Figs. 8(c) and (d) with those in Figs. 8(a) and (b), respectively, it is seen that the size of the indentation zone increases with an increasing indentation depth.

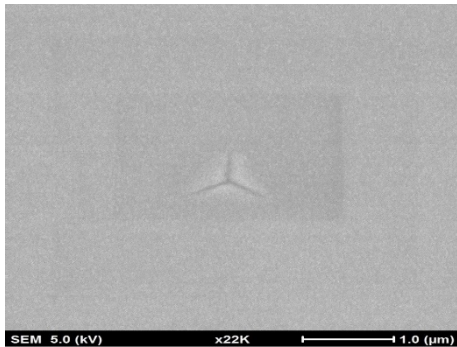


Fig. 8 (a) Surface topographies of indented as-deposited specimen with 200 nm thickness and indentation depth of 150 nm obtained by SEM.

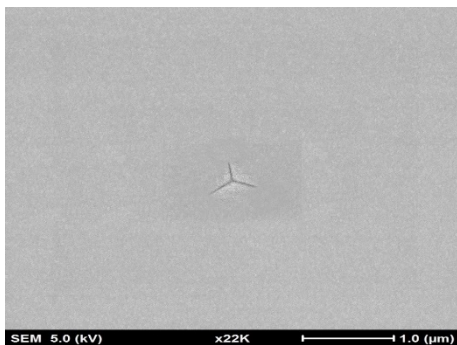


Fig. 8 (b) Surface topographies of indented annealed specimen with 200 nm thickness and indentation depth of 150 nm obtained by SEM.

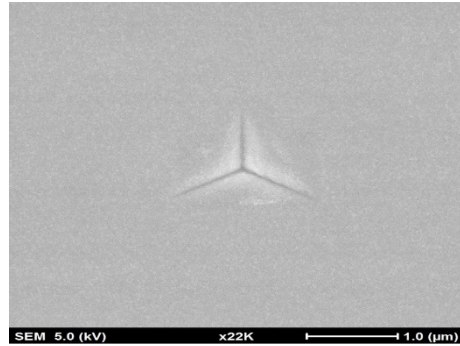


Fig. 8 (c) Surface topographies of indented as-deposited specimen with 200 nm thickness and indentation depth of 250 nm obtained by SEM.

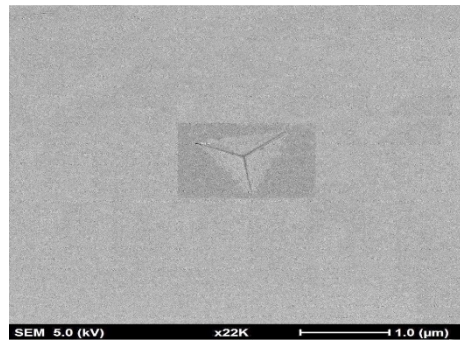


Fig. 8 (d) Surface topographies of indented annealed specimen with 200 nm thickness and indentation depth of 250 nm obtained by SEM.

Figures 9(a) and (b) show the SEM surface topographies of the as-deposited and annealed samples, respectively, with a film thickness of 300 nm and an indentation depth of 150 nm.

Figures 9(c) and (d) show the corresponding images for the same film thickness of 300 nm, but a higher indentation depth of 350 nm. As for the thin films with a smaller thickness of 200 nm, the size of the indentation zone increases with an increasing indentation depth, but decreases in the annealed condition.

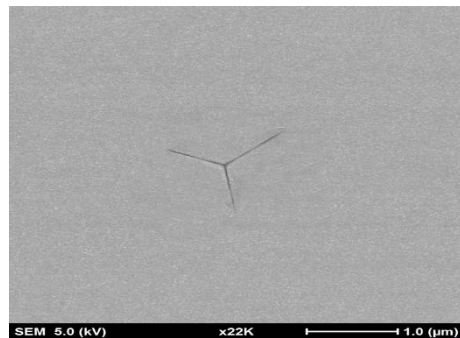


Fig. 9 (a) Surface topographies of indented as-deposited specimen with 300 nm thickness and indentation depth of 150 nm obtained by SEM.

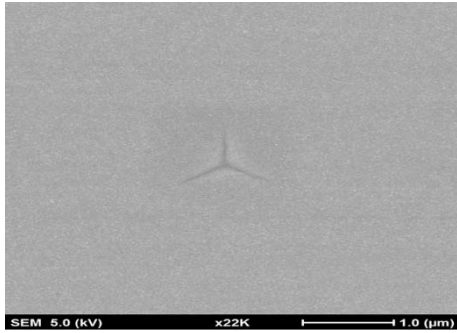


Fig. 9 (b) Surface topographies of indented annealed specimen with 300 nm thickness and indentation depth of 150 nm obtained by SEM.

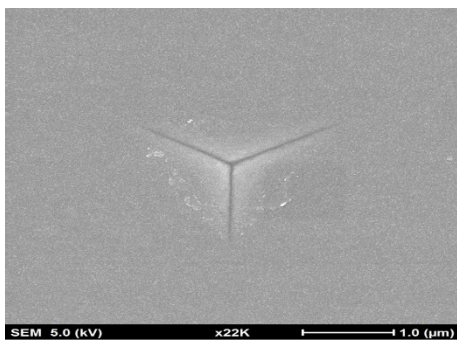


Fig. 9 (c) Surface topographies of indented as-deposited specimen with 300 nm thickness and indentation depth of 350 nm obtained by SEM.

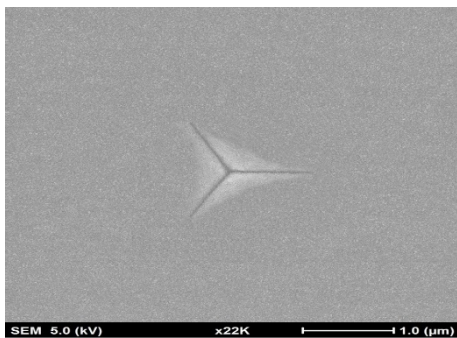


Fig. 9 (d) Surface topographies of indented annealed specimen with 300 nm thickness and indentation depth of 350 nm obtained by SEM.

Comparing the images presented in Fig. 9 with those shown in Fig. 8, it is seen that the size of the indentation zone increases with an increasing film thickness. Overall, the results presented in Figs. 8 and 9 show that the size of the indentation area increases with an increasing film thickness and indentation depth, but decreases following annealing.

TEM analysis

Figures 10(a) and (b) present TEM micrographs of the as-deposited and annealed specimens, respectively, with a film thickness of 200 nm and an indentation depth of 150 nm. A well-defined boundary is observed between the CuO film and the GaAs substrate in both cases.

As shown in the selected area (electron) diffraction (SAED) pattern in Fig. 10(c), the as-deposited and annealed CuO film has a polycrystalline structure, while the GaAs substrate has a single crystal structure (Fig. 10(d)).

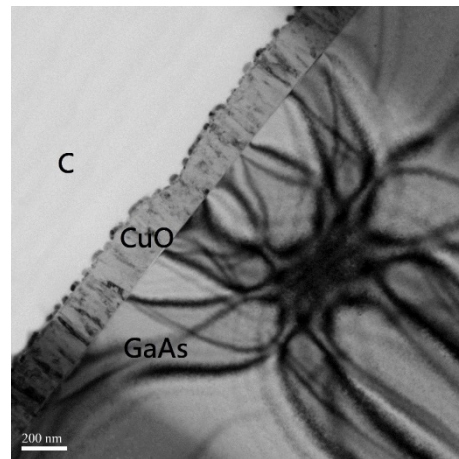


Fig. 10 (a) Micrographs of indented as-deposited specimen with 200 nm thickness and indentation depth of 150 nm obtained by TEM.

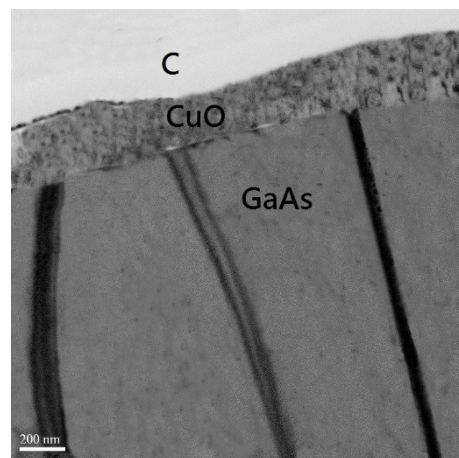


Fig. 10 (b) Micrographs of indented annealed specimen with 200 nm thickness and indentation depth of 150 nm obtained by TEM.

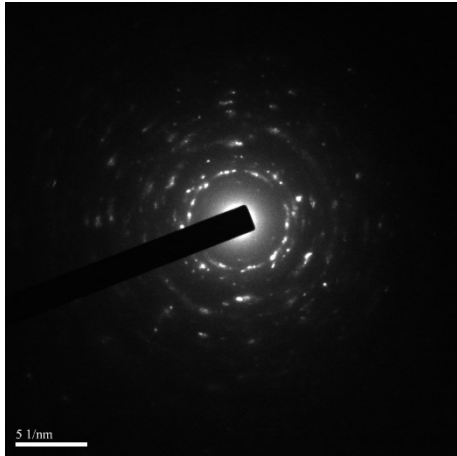


Fig. 10 (c) Selected area electron diffraction (SAED) patterns of CuO film.

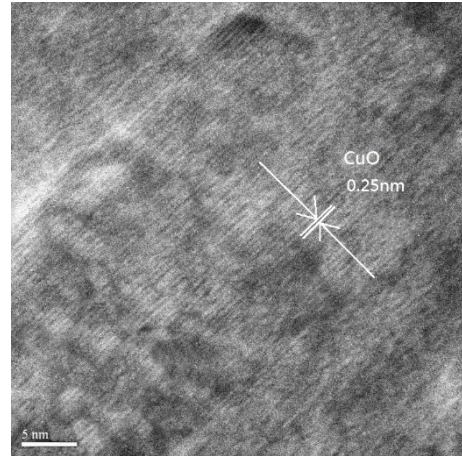


Fig. 10 (e) High-resolution TEM (HRTEM) micrographs of: CuO film.

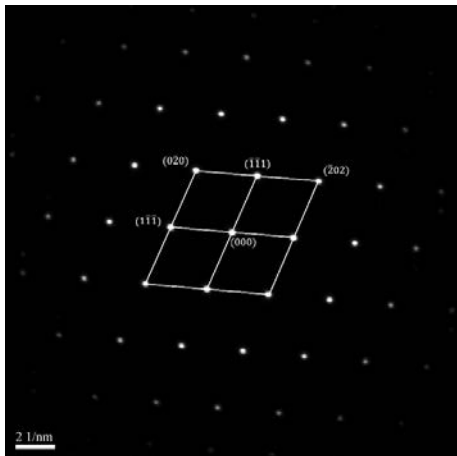


Fig. 10 (d) Selected area electron diffraction (SAED) patterns of GaAs substrate.

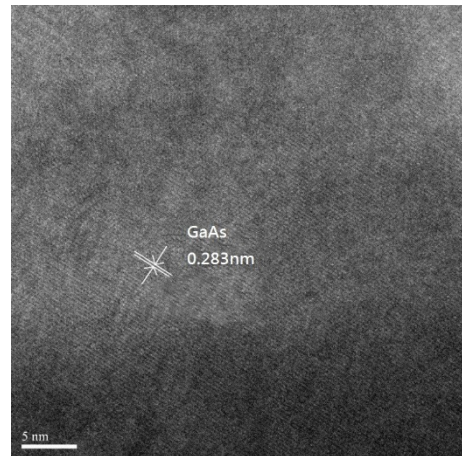


Fig. 10 (e) High-resolution TEM (HRTEM) micrographs of: GaAs substrate.

Figures 10(e) and (f) present high-resolution TEM (HRTEM) micrographs of the as-deposited and annealed CuO film and GaAs substrate, respectively. The lattice spacing of the CuO film is found to be around 0.25 nm, while that of the GaAs substrate is approximately 0.283 nm. It is noted that these two lattice spacings are consistent with the findings of (Tan *et al*, 2007) and (Bum, 1988).

Figures 11(a) and (b) show the TEM micrographs of the as-deposited and annealed samples, respectively, with the same film thickness of 200 nm, but a higher indentation depth of 250 nm. It is seen that the crystal structures of the CuO film and GaAs substrate are similar to those of the samples indented to a lower depth of 150 nm. However, a delamination effect is observed at the interface between the CuO film and the GaAs substrate in both the as-deposited condition and the annealed condition under the higher indentation depth of 250 nm.

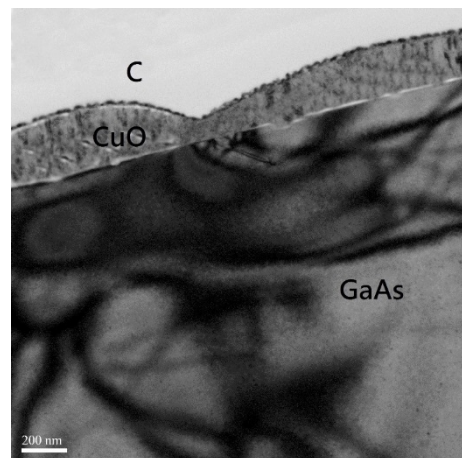


Fig. 11 (a) Micrographs of indented as-deposited specimen with 200 nm thickness and indentation depth of 250 nm obtained by TEM.

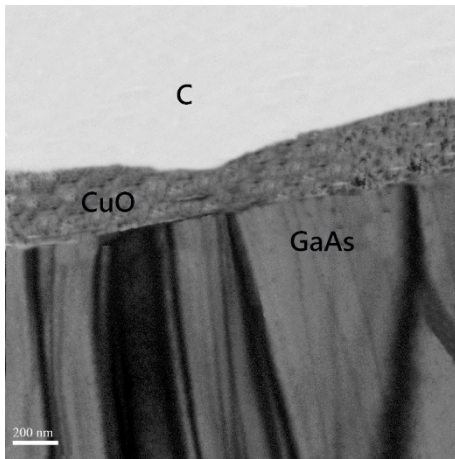


Fig. 11 (b) Micrographs of indented annealed specimen with 200 nm thickness and indentation depth of 250 nm obtained by TEM.

Figures 12(a) and (b) show the TEM micrographs of the as-deposited and annealed samples, respectively, with a thickness of 300 nm and an indentation depth of 150 nm.

Figures 12(c) and (d) present the equivalent micrographs for a greater indentation depth of 350 nm.

As shown, the CuO film again has a polycrystalline structure, while the GaAs substrate has a single crystal structure. However, compared to the thin films with a thickness of 200 nm, delamination occurs only in the as-deposited specimens and becomes more severe as the indentation depth is increased. Finally, dislocation clusters are observed only on the GaAs substrate of the annealed specimen indented to a maximum depth of 350 nm. Overall, the results presented in Figs. 11 and 12 show that the delamination behaviour depends strongly on the indentation depth, the thin film thickness, and the annealing condition.

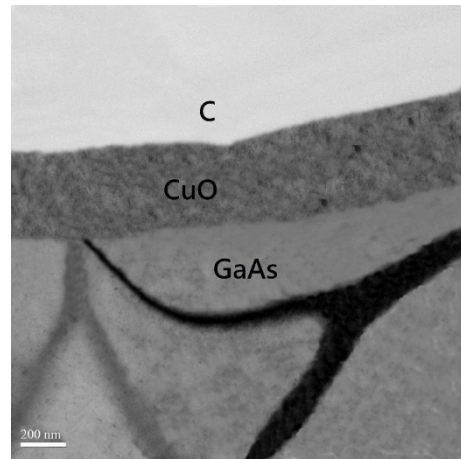


Fig. 12 (b) Micrographs of indented annealed specimen with 300 nm thickness and indentation depth of 150 nm obtained by TEM.

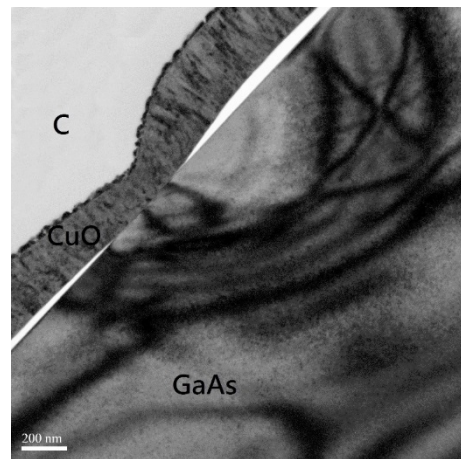


Fig. 12 (c) Micrographs of indented as-deposited specimen with 300 nm thickness and indentation depth of 350 nm obtained by TEM.

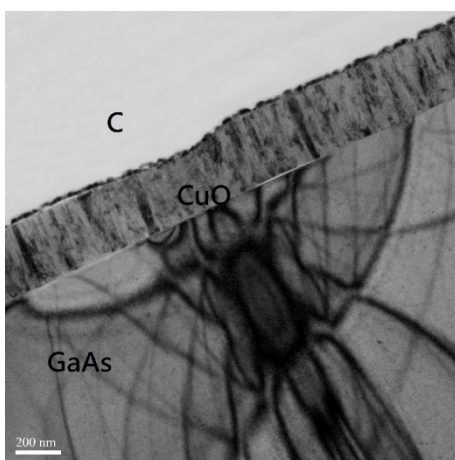


Fig. 12 (a) Micrographs of indented as-deposited specimen with 300 nm thickness and indentation depth of 150 nm obtained by TEM.

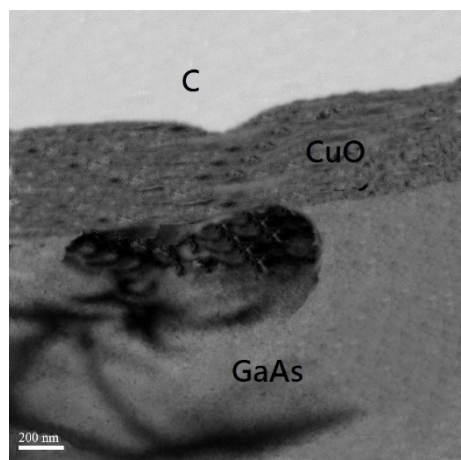


Fig. 12 (d) Micrographs of indented annealed specimen with 300 nm thickness and indentation depth of 350 nm obtained by TEM.

CONCLUSIONS

This study has investigated the nanoindentation behaviour of as-deposited and annealed CuO/GaAs thin-film systems with film thicknesses of 200 nm and 300 nm, respectively, and various indentation depths in the range of 150 nm to 350 nm. The results have shown that a pop-in event occurs in the loading curve of all the as-deposited specimens, irrespective of the film thickness or indentation depth. However, for the annealed specimens, the loading curves are all smooth and continuous with no pop-in features. For both the as-deposited specimens and the annealed specimens, the maximum load increases with an increasing film thickness and indentation depth. Furthermore, the hardness and Young's modulus are insensitive to the film thickness and indentation depth, but reduce slightly following annealing. The SEM images have shown that for both the as-deposited samples and the annealed samples, the indentation area increases with an increasing indentation depth and thin film thickness. However, for a given indentation depth and film thickness, the indentation area reduces in the annealed condition. Moreover, the TEM observations have revealed that delamination occurs at the interface between the CuO film and the GaAs substrate for all of the samples other than the annealed samples with a thin film thickness of 300 nm. Dislocations within the GaAs substrate microstructure have been observed only in the annealed sample with a film thickness of 300 nm and an indentation depth of 350 nm. The SAED patterns have revealed that the as-deposited and annealed CuO film has a polycrystalline structure, while the GaAs substrate has a single crystal structure. Finally, the high-resolution TEM (HRTEM) images have shown that the CuO film and GaAs substrate have lattice spacings of 0.25 nm and 0.283 nm, respectively.

ACKNOWLEDGMENT

The authors gratefully acknowledge the financial support provided to this study by the Ministry of Science and Technology (MOST) of Taiwan under Contract No. MOST 108-2221-E-006-190.

REFERENCES

- A. J. Haq, P. Munroe, M. Hoffman, P. Martin, and A. Bendavid, "Deformation behaviour of DLC coatings on (111) silicon substrates," *Thin Solid Films*, vol. 516, no. 2-4, pp. 267-271, 2007.
- D. Chrobak, K. Nordlund, and R. Nowak, "Nondislocation origin of GaAs nanoindentation pop-in event," *Phys Rev Lett*, vol. 98, p. 045502, Jan 26 2007.
- E. P. S. Tan, Y. Zhu, T. Yu, L. Dai, C. H. Sow, V. B. C. Tan and C. T. Lim, "Crystallinity and surface effects on Young's modulus of CuO nanowires", *APPLIED PHYSICS LETTERS* 90, 163112 (2007).
- G. Huajian, C. Cheng-Hsin, and L. Jin, "Elastic contact versus indentation modeling of multi-layered materials," *International Journal of Solids and Structures*, vol. 29, pp. 2471-2492, 1992.
- G. M. Pharr, W. C. Oliver, and F. R. Brotzen, "On the generality of the relationship among contact stiffness, contact area, and elastic modulus during indentation," *Journal of Materials Research*, vol. 7 No.3, 1992.
- G. Patriarche, E. Le Bourhis, D. Faurie, and P. O. Renault, "TEM study of the indentation behaviour of thin Au film on GaAs," *Thin Solid Films*, vol. 460, pp. 150-155, 7/22/ 2004.
- H. S. Leipner, D. Lorenz, A. Zeckzer, H. Lei, and P. Grau, "Nanoindentation pop-in effect in semiconductors," *Physica B: Condensed Matter*, vol. 308-310, pp. 446-449, 12// 2001.
- Int.J.Electrochem, "Annealing Effects on the Properties of Copper Oxide Thin Films Prepared by Chemical Deposition", *Sci.*, 6 (2011) 6094 – 6104.
- I. Manika and J. Maniks, "Size effects in micro- and nanoscale indentation," *Acta Materialia*, vol. 54, pp. 2049-2056, 2006.
- K. K. Bum, "Interfacial reactions in the Ti/GaAs system," *Journal of Vacuum Science & Technology A: Vacuum, Surfaces, and Films*, vol. 6, no. 3, p. 1473, 1988.
- K. Wasmer, R. Gassilloud, J. Michler, and C. Ballif, "Analysis of onset of dislocation nucleation during nanoindentation and nanoscratching of InP, " *Journal of Materials Research*, vol. 27, no. 01, pp. 320-329, 2011.
- M. Hansen and K. Anderko, "Constitution of Binary Alloys," 2nd ed. McGraw-Hill, N. Y. (1958) 51.
- Nau-Hung Tsao, "The effect of CuOx thin film oxidation state on the enhancement of hole transportation in the inverted polymer solar cell. ",2011.
- R. Rao, J. E. Bradby, S. Ruffell, and J. S. Williams, "Nanoindentation-induced phase transformation in crystalline silicon and relaxed amorphous silicon," *Microelectronics Journal*, vol. 38, pp. 722-726, 2007.
- S. Timoshenko and J. N. Goodier, "Theory of Elasticity," 2nd ed. McGraw-Hill, N. Y., 1951.
- S. Yugang, K. Seiyon, A. Ilesanmi, and R. J. A, "Bendable GaAs metal-semiconductor field-effect transistors formed with printed GaAs wire arrays on plastic substrates," *Applied Physics Letters*, vol. 87, p. 083501, 2005.
- T. Nakamura, "Mars Rover power system for solar and laser beam Utilization," *Concepts and Approaches for Mars Exploration*, 2012.
- W. C. Oliver and G. M. Pharr, "An improved technique for determining hardness and elastic modulus using load and displacement sensing indentation experiments," *Journal of Materials*

- Research*, vol. 7, pp. 1564-1583, 1992.
- X. Li and B. Bhushan, "A review of nanoindentation continuous stiffness measurement technique and its applications," *Materials characterization*, vol. 48, no. 1, pp. 11-36, 2002.
- Yatendra S. Chaudhary, Anshul Agrawala, Rohit Shrivastav, Vibha R. Satsangi, Sahab Dass, "A study on the photoelectrochemical properties of copperoxide thin films", *International Journal of Hydrogen Energy* 29 (2004) 131 – 134.
- Y. Cao, S. Allameh, D. Nankivil, S. Sethiaraj, T. Otiti, and W. Soboyejo, "Nanoindentation measurements of the mechanical properties of polycrystalline Au and Ag thin films on silicon substrates: Effects of grain size and film thickness," *Materials Science and Engineering: A*, vol. 427, no. 1-2, pp. 232-240, 2006.

0.25nm 和0.283nm。

退火在氧化銅/砷化鎵薄膜 奈米壓痕行為上之效應分 析

李偉賢 張家源

國立成功大學機械工程學系

摘要

本研究主要是探討退火在銅/砷化鎵薄膜系統之奈米壓痕行為及薄膜顯微結構上的效應。本實驗首先利用電子束蒸鍍法在砷化鎵晶圓上製作200 nm及300nm厚度之銅薄膜，經過退火處理，條件為加熱至500°C，並持溫30分鐘，再分別對200nm試片進行150nm 及250 nm深度；對300nm試片進行150nm 350 nm深度之奈米壓痕試驗，藉以瞭解退火對奈米壓痕行為及微觀結構之影響。奈米壓痕試驗結果顯示，硬度及楊氏模數受退火影響甚鉅，退火前及退火後之硬度-深度曲線有很大的不同，且在最大壓深下，退火後的硬度值較未退火的低。楊氏模數則有相同的趨勢。負載-深度曲線顯示在對200nm試片進行150nm 及250 nm深度；及對300nm試片進行150nm 350 nm深度時，退火與未退火的荷載曲線皆有pop-in的現象發生；而所有的卸載曲線則都是連續而無pop-out的現象發生。掃描式電子顯微鏡之觀測結果顯示，壓痕的區域隨著壓痕深度及薄膜厚度的增加而增加。穿透式電子顯微鏡之觀測結果證實，薄膜的分離僅發生在膜厚300 nm，壓深150 nm與350 nm。而差排僅形成於膜厚300 nm，壓深350 nm之退火試片。為結構分析證實CuO薄膜是屬多晶結構，而GaAs為單晶結構。高解析穿透式電子顯微鏡分析顯示，CuO薄膜和GaAs 基材的晶格間距分別為